Application of a continuum constitutive model to metallic foam DEN-specimens in compression

Onck, P.R.

Published in:
International Journal of Mechanical Sciences

DOI:
10.1016/S0020-7403(01)00060-1

Publication date:
2001

PERGAMON International Journal of Mechanical Sciences 43 (2001) 2947–2959

International Journal of MECHANICAL SCIENCES

www.elsevier.com/locate/ijmecsci

Application of a continuum constitutive model to metallic foam DEN-specimens in compression

P.R. Onck *

Koiter Institute Delft, Delft University of Technology, Mekelweg 2, 2628 CD Delft, The Netherlands

Received 11 August 2000; received in revised form 16 March 2001

Abstract

The behavior of double-edge notched specimens of metallic foams in compression is studied numerically. To model the constitutive behavior of the metallic foam, a recently developed phenomenological, pressure-sensitive yield surface [1] is used. Compressive yielding in response to hydrostatic stress is incorporated through a dependence on the plastic Poisson ratio v^p. Results are presented in terms of limit load F_{lim}, as a function of notch depth, a/W, and the plastic Poisson ratio v^p. For incompressible plastic behavior, $v^p = 0.5$, the results show notch-strengthening due to constrained plastic deformation near the crack/notch-tip. For fully compressible plastic behavior (no lateral expansion on uniaxial compression, $v^p = 0$), no notch-effect is observed. The validity of using a continuum model for the analysis of metallic foam notched specimens is discussed.

Keywords: Metallic foams; Cellular materials; Finite element method; Constitutive equations

1. Introduction

Metallic foams have high strength and stiffness at a relatively low density, which make them attractive for ultralight structural applications. The advent of novel production techniques to make better and cheaper foams, in combination with an increased understanding of the thermomechanical properties has enhanced their potential of becoming a new class of engineering materials [2]. For the safe design of structural components, knowledge must be provided concerning their mechanical performance in the presence of holes, notches and cracks. To gain an understanding of the behavior of metallic foams in non-uniform, multiaxial stress fields, this paper analyzes the compressive behavior of double edge-notched (DEN) specimens.

* Tel.: +31-15-278-6833; fax: +31-15-278-2150.
E-mail address: p.r.onck@wbmt.tudelft.nl (P.R. Onck).

0020-7403/01/$ - see front matter
PII: S0020-7403(01)00060-1

The compressive stress–strain curve of open-cell metal foams shows linear elasticity at low strains, caused by the bending of cell walls. At higher strains, plastic hinges form in the cell walls, causing the cells to collapse, which results in a long collapse plateau (increasing strain at constant stress). Finally, the foam densifies, resulting in a steep rise of the stresses. In case of closed-cell foams the above mechanisms are accompanied by cell face stretching in the elastic regime and by face yielding during collapse. Theoretical models predict a much stiffer and stronger response for closed-cell foams, due to the fact that stretching is the dominant deformation mode as compared to bending in the open-cell foams [3]. However, experiments show a large "knock-down factor" for closed-cell foams which is attributed to irregularities (cell wall wiggles, cell face corrugations) and imperfections (cracks in cell faces, missing cell walls) in the cellular microstructure [4–6], promoting bending to be the dominant deformation mode [7,8]. This is also reflected in the multi-axial stress response of metallic foams, where it is found that the hydrostatic yield stress is of similar magnitude to the uniaxial yield stress.

Recently, much effort has been put in the development of a constitutive model for metallic foams, because of its obvious importance in the engineering analysis of applications and design methods. Based on multi-axial yield data (e.g. [1,9,10]), several phenomenological constitutive models have been proposed (e.g. [1,11–13]). Characteristic experimental phenomena included in these descriptions are the hydrostatic stress dependence of yielding, the extreme hardening behavior at large compressive strains and the limited lateral expansion on uniaxial compression (i.e. small plastic Poisson ratio). Recently, Miller [13] used such a constitutive model to numerically explore notch effects for one specific notch depth as well as indentation of foam cores with and without dense face sheets. Sugimura et al. [7] already performed a preliminary investigation of the hydrostatic stress dependence of notch compression tests. They observed an increased resistance to yielding with increasing notch depth when the yield strength in hydrostatic compression is much larger than in shear. In the current paper, we explore notch effects in some more detail by adopting a recently developed material model for foams in which the shape of the yield surface is directly related to the plastic Poisson ratio [1]. This enables a quantitative relation between the notch-strengthening effect and measured values of the plastic Poisson ratio.

The paper is organized as follows. Section 2 contains an overview of the constitutive model for metallic foams, the DEN specimen geometry and some details concerning the numerical implementation. In Section 3, the results are shown in terms of overall response (Section 3.1) and local deformation patterns (Section 3.2). Finally, the validity of using a continuum model for the analysis of notched specimens is discussed in Section 4.

2. Numerical model

In this section, the numerical model is presented. The constitutive law is summarized in Section 2.1, followed by a description of the specimen geometry and boundary conditions in Section 2.2. For the implementation of the model the commercial finite element package ABAQUS is used.

2.1. Foam constitutive law

To model the deformation behavior of the metallic foam we adopt the phenomenological constitutive law developed by Deshpande and Fleck [1]. A summary of the model is given below.

Employing the fact that foams yield in response to both hydrostatic loading as well as deviatoric loading, a yield surface is defined by

$$\Phi \equiv \hat{\sigma} - Y = 0, \tag{1}$$

where Y is the yield stress and $\hat{\sigma}$ is an equivalent stress measure defined as

$$\hat{\sigma}^2 = \frac{1}{[1 + (\alpha/3)^2]}(\sigma_e^2 + \alpha^2 \sigma_m^2) \tag{2}$$

with $\sigma_e = (\frac{3}{2}\sigma'_{ij}\sigma'_{ij})^{1/2}$ the von Mises effective stress, σ'_{ij} the Cartesian components of the stress deviator and $\sigma_m = \frac{1}{3}\sigma_{kk}$ the mean stress. Clearly, (1) defines an ellipse in (σ_m, σ_e) space, with its shape determined by the phenomenological parameter α. One of the attractive features of this yield surface is that the parameter α can be linked to the plastic Poisson ratio v^p in a uniaxial compression test:

$$v^p = -\frac{\dot{\varepsilon}^p_{11}}{\dot{\varepsilon}^p_{22}} = \frac{(1/2) - (\alpha/3)^2}{1 + (\alpha/3)^2}, \tag{3}$$

where $\dot{\varepsilon}^p_{11}$ and $\dot{\varepsilon}^p_{22}$ are the plastic strain rate perpendicular and parallel to the direction of compression, respectively. For $\alpha = \sqrt{4.5}$ we have $v^p = 0$, meaning that no lateral expansion will occur upon compressing the specimen uniaxially. For $\alpha = 0$ we have $v^p = 0.5$, corresponding to incompressible plasticity, $\hat{\sigma}$ reduces to σ_e and J_2 flow theory is recovered. Note that the plastic Poisson ratio increases with relative density, such that $v^p = 0.5$ no longer corresponds to a metallic foam, but to the limit of a dense metal. Typical values for the plastic Poisson ratio for low-density foams are in the range between 0 and 2.5. Gioux et al. [10] report $v^p = 0.052$ for an open-cell foam (Duocel, 7% relative density) and $v^p = 0.024$ for a closed-cell foam (Alporas, 8%). Deshpande and Fleck [1] report slightly different values: $v^p = 0.013$ (Alporas, 8.4%), $v^p = 0.174$ (Duocel, 7%) and $v^p = 0.247$ (Alporas, 13%).

Assuming associated flow and using consistency of plastic loading, the plastic strain rate can be written as

$$\dot{\varepsilon}^p_{ij} = \frac{\dot{Y}}{H}\frac{\partial \Phi}{\partial \sigma_{ij}} \tag{4}$$

with H the hardening modulus related to $\dot{\hat{\varepsilon}}$, the plastic work rate-conjugate to $\hat{\sigma}$, by

$$H = \frac{\dot{\hat{\sigma}}}{\dot{\hat{\varepsilon}}}. \tag{5}$$

The equivalent strain rate $\dot{\hat{\varepsilon}}$ can be expressed in terms of the effective plastic strain rate $\dot{\varepsilon}_e = (\frac{2}{3}\dot{\varepsilon}'^p_{ij}\dot{\varepsilon}'^p_{ij})^{1/2}$ and the volumetric plastic strain rate $\dot{\varepsilon}_m = \dot{\varepsilon}^p_{kk}$ as

$$\dot{\hat{\varepsilon}}^2 = \left[1 + \left(\frac{\alpha}{3}\right)^2\right]\left(\dot{\varepsilon}_e^2 + \frac{1}{\alpha^2}\dot{\varepsilon}_m^2\right). \tag{6}$$

It is assumed that hardening is isotropic so that the yield surface as given by Eqs. (1) and (2) evolves in a self-similar manner. The hardening modulus H is obtained from a uniaxial compression test for which $\hat{\sigma}$ reduces to the applied Cauchy stress σ and $\hat{\varepsilon}$ to the uniaxial compressive logarithmic plastic strain ε. Then, H is the slope of the Cauchy stress-logarithmic strain curve at strain level ε:

$$H(\varepsilon) = \frac{\dot{\sigma}}{\dot{\varepsilon}}. \tag{7}$$

The hardening response is deduced from a uniaxial compression test typical for an Alporas closed-cell metallic foam [14], which is given as input to ABAQUS. Figs. 1a and b show the uniaxial response at small and large strains, respectively. We account for the characteristic behavior of Alporas, showing a negligibly short elastic region ($E = 1.15$ GPa, $v = 0.33$) after which yielding starts very early (at $\sigma \approx 0.2$) due to local plastic hinge formation at cell nodes (see [8]). This behavior is emphasized in Fig. 1a by showing the unloading modulus which is much larger than the slope of the stress–strain curve before reaching the plateau stress. After the plateau stress, σ_0, is reached at $\sigma_0 = 1.3$ MPa the material starts to densify at a compressive logarithmic strain $\varepsilon \approx 2$, resulting in extreme hardening (see Fig. 1b). A user-defined material subroutine (UMAT) of the constitutive model is used, implemented by Chen [15].

2.2. Specimen geometry and boundary conditions

Double-edge notched specimens are analyzed, where $a/2$ denotes the notch length, B the ligament width, $W = a + B$ the width of the specimen, ρ the notch tip radius and h the height of the specimen. Only a quarter of the DEN specimen is analyzed, employing symmetry. A typical finite element mesh including dimensions and displacement boundary conditions is shown in Fig. 2. Symmetry boundary conditions are applied along the symmetry line and the ligament, a uniform negative displacement $-U$ is prescribed at the top of the specimen, while the rest of the boundary degrees of freedom are stress-free. Plane strain conditions are assumed. A finite strain formulation is adopted, using 8-noded quadratic elements for most cases, while for cases with incompressible plasticity, hybrid versions are used to circumvent volumetric locking. Convergence was checked by comparing results for different mesh densities.

3. Results

In this section, we analyze the compressive behavior of metallic foam DEN-specimens by focusing on the effect of a/W and v^p, while keeping ρ/W and h/W fixed.

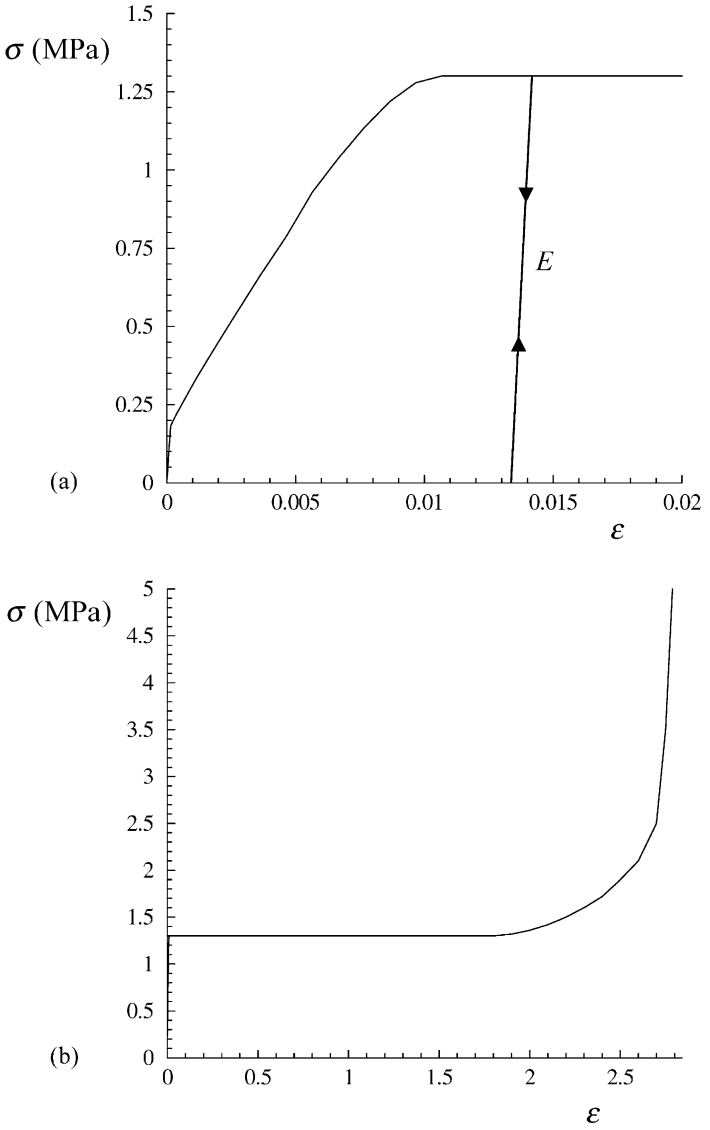

Fig. 1. The uniaxial Cauchy stress—logarithmic strain curve. (a) At small strains. The elastic (unloading) modulus E is shown; (b) at large strains.

3.1. Overall response

Fig. 3 shows the overall response of a specimen with geometry $a/W = 0.5$, $h/W = 1.5$ and $2\rho/W = 0.05$. The total applied compressive force per unit (out-of-plane) thickness F, normalized by the width W, is plotted against the compressive logarithmic strain measure

$$\varepsilon = -\ln\left(\frac{h-U}{h}\right) \tag{8}$$

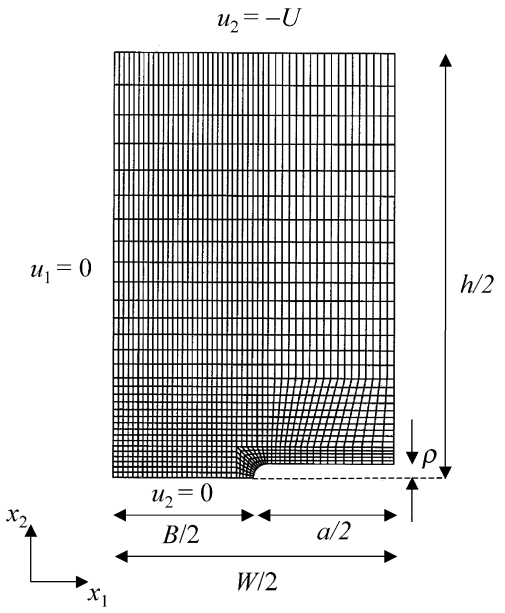

Fig. 2. Typical finite element mesh, including dimensions and displacement boundary conditions.

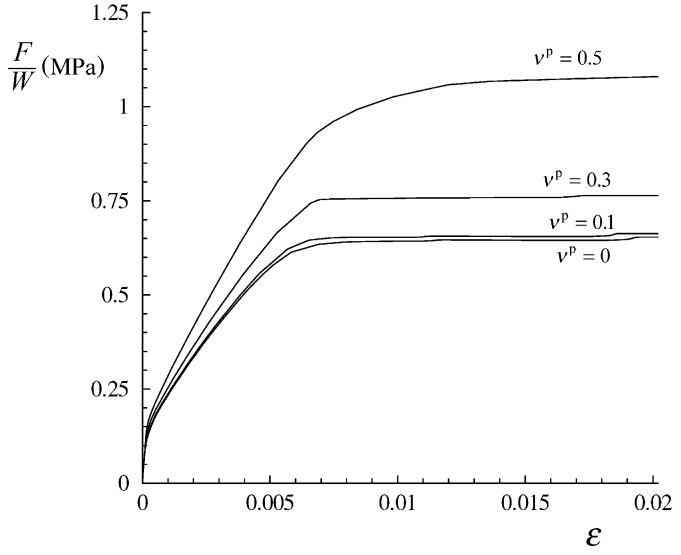

Fig. 3. Force per unit length divided by the width, $F_{\lim}/W$, as a function of logarithmic compressive strain ε, for different values of the plastic Poisson ratio ν^p. Note that $\nu^p = 0.5$ no longer corresponds to a metallic foam, but to a dense metal.

with h the initial height of the specimen. Results are shown for different plastic Poisson ratios ν^p (introduced by the parameter α in the yield surface through Eq. (3)) ranging from pure crushing, $\nu^p = 0$, to incompressible behavior, $\nu^p = 0.5$ (dense metal). At $\varepsilon = 0.015$ the maximum load that the specimen can carry has been reached. Clearly, this limit load, $F_{\lim}$, increases with

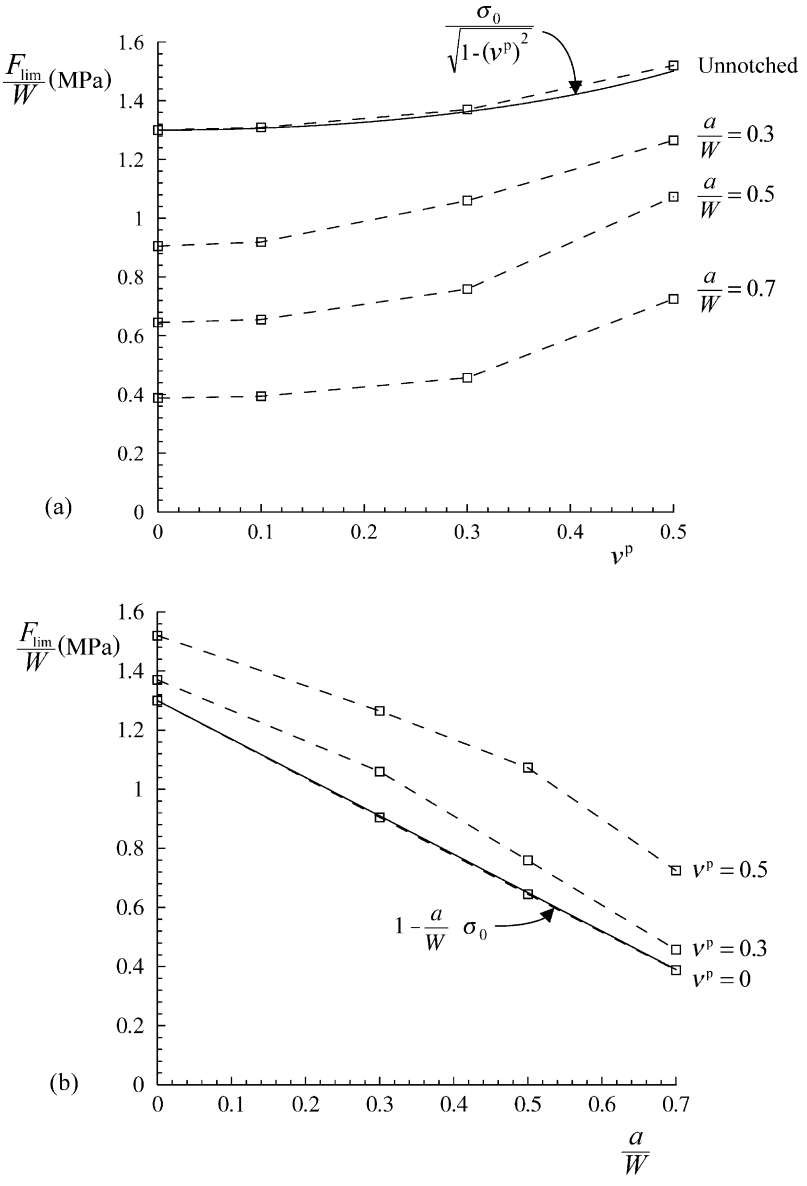

Fig. 4. (a) Limit load over specimen width, F_{lim}/W, as a function of plastic Poisson ratio ν^p, for different notch depths a/W; (b) same data as in (a), but plotted as a function of a/W for different ν^p.

plastic Poisson ratio which is attributed to the higher constraint on plastic deformation, imposed by the reduced material compressibility (see also [13]).

Next, we focus on the limit loads, F_{lim}/W, only and compare results for different notch depths a/W as a function of ν^p (see Fig. 4a). The other cases ($a/W = 0.3$ and 0.7) are generated by varying a only, so that the dimensionless parameters $2\rho/W$ and h/W remain unchanged. Also, the result for an unnotched specimen is shown, which is similar to a plane strain uniaxial

compression test. Clearly, applying plane strain boundary conditions alone, already accounts for an increase in the limit load as v^p increases, due to the out-of-plane constraint. An exact expression for this effect can be derived as follows. Picture a plane strain-stress state. To calculate the out-of-plane stress σ_{33} in terms of the in-plane stresses, we use the plane strain condition $\dot{\varepsilon}^p_{33} = 0$ in Eq. (4), which results in (see also [15])

$$\frac{\partial \Phi}{\partial \sigma_{33}} = \frac{1}{1 + (\alpha/3)^2} \left[\frac{3}{2} \frac{\sigma'_{33}}{\hat{\sigma}} + \frac{\alpha^2}{3} \frac{\sigma_m}{\hat{\sigma}} \right] = 0. \tag{9}$$

Solving this equation for σ_{33} yields

$$\sigma_{33} = \frac{((1/2) - (\alpha^2/9))}{(1 + (\alpha^2/9))} [\sigma_{11} + \sigma_{22}] = v^p [\sigma_{11} + \sigma_{22}]. \tag{10}$$

For uniaxial tension we have $\sigma_{11} = 0$, $\sigma_{22} = \sigma$, $\sigma_{33} = v^p \sigma$. Substitution in Eqs. (1) and (2) and assuming that yielding occurs at the plateau stress σ_0, results in

$$\sigma_{lim} = \frac{\sigma_0}{\sqrt{1 - (v^p)^2}}. \tag{11}$$

This expression is plotted against the numerical results in Fig. 4a with $\sigma_0 = 1.3$ MPa and is shown to agree well. Note that the dashed lines merely serve to connect numerical data points for clarity, while the solid line is an independent function (11). Clearly, increasing the notch depth (a/W) decreases the net-section-area, which increases the net-section-stress and thus reduces the load carrying capacity, F_{lim}/W (Fig. 4a). The same data are plotted in Fig. 4b as a function of a/W for $v^p = 0$, 0.3 and 0.5. An estimate for the limit load is

$$\frac{F_{lim}}{W} = \left(1 - \frac{a}{W}\right) \sigma_0, \tag{12}$$

which is plotted with $\sigma_0 = 1.3$ MPa in Fig. 4b by a solid line. The notch effect for $v^p = 0$ is fully captured by this simple net-section-stress argument, while for $v^p > 0$ strengthening occurs with respect to the $v^p = 0$ case.

To eliminate the net-section-stress effect we normalize the limit force F_{lim} by the ligament length $B = a - W$. The value F_{lim}/B is a measure for the net-section stress needed to crush the ligament. Fig. 5a explicitly shows the notch-strengthening effect. For $v^p = 0$ and 0.1, the material in the ligament does not feel the presence of the notches, since the limit force is the same for all a/W. For $v^p = 0.3$ some notch strengthening takes place, although the notch depth does not play a role. Finally, for $v^p = 0.5$ we have a dense solid instead of a foam. Then, also the notch depth enters the problem and the limit load increases with notch depth. To obtain a simple estimate of this notch-strengthening behavior we focus on a general plane strain biaxial stress state $\sigma_{11} = t\sigma_{22}$ ($0 < t < 1$), $\sigma_{22} = \sigma$, $\sigma_{12} = 0$. The out-of-plane stress σ_{33} follows from Eq. (10). The parameter t is introduced to incorporate the effect of the notches on the stress triaxiality. Substitution of this stress state in Eqs. (1) and (2) and equating $\hat{\sigma}$ to the plateau stress σ_0 yields

$$\sigma_{lim} = \frac{\sigma_0}{\sqrt{2/3(1 + v^p)[3/2(t+1)^2(1 - v^p) - 3t]}}. \tag{13}$$

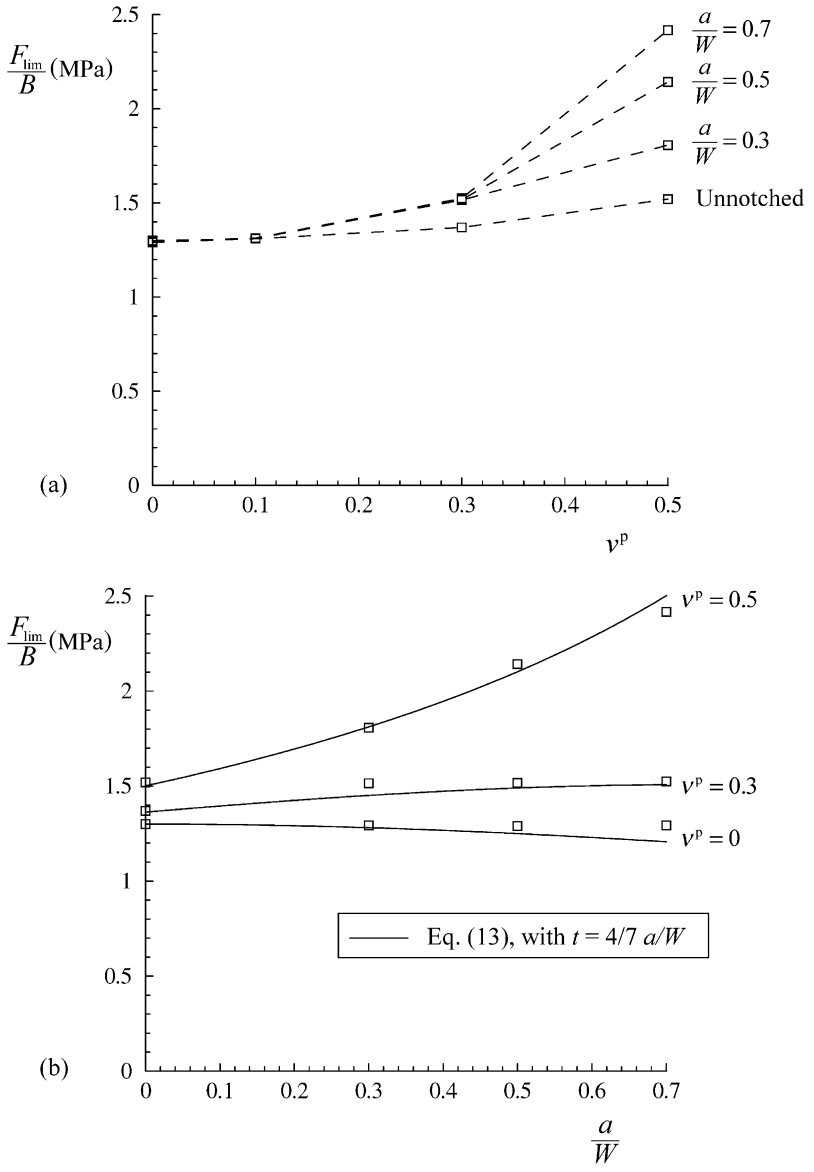

Fig. 5. (a) Limit load over ligament width, $F_{\lim}/B$, as a function of plastic Poisson ratio ν^p, for different notch depths a/W; (b) same data as in (a), but plotted as a function of a/W for different ν^p. The numerical data points are compared with Eq. (13), with $t = 4/7\ a/W$.

For $t = 0$, no notch is present and (13) reduces to (11), while for notched specimens it is assumed that the triaxiality parameter t scales linearly with a/W: $t = ca/W$, where the constant c is fit to be 4/7. Substituting this into (13) yields an expression for $\sigma_{\lim}$ as a function of ν^p and a/W. This approximate expression for the notch-strengthening effect is plotted in Fig. 5b and compared with the results of Fig. 5a, which are now shown as a function of a/W

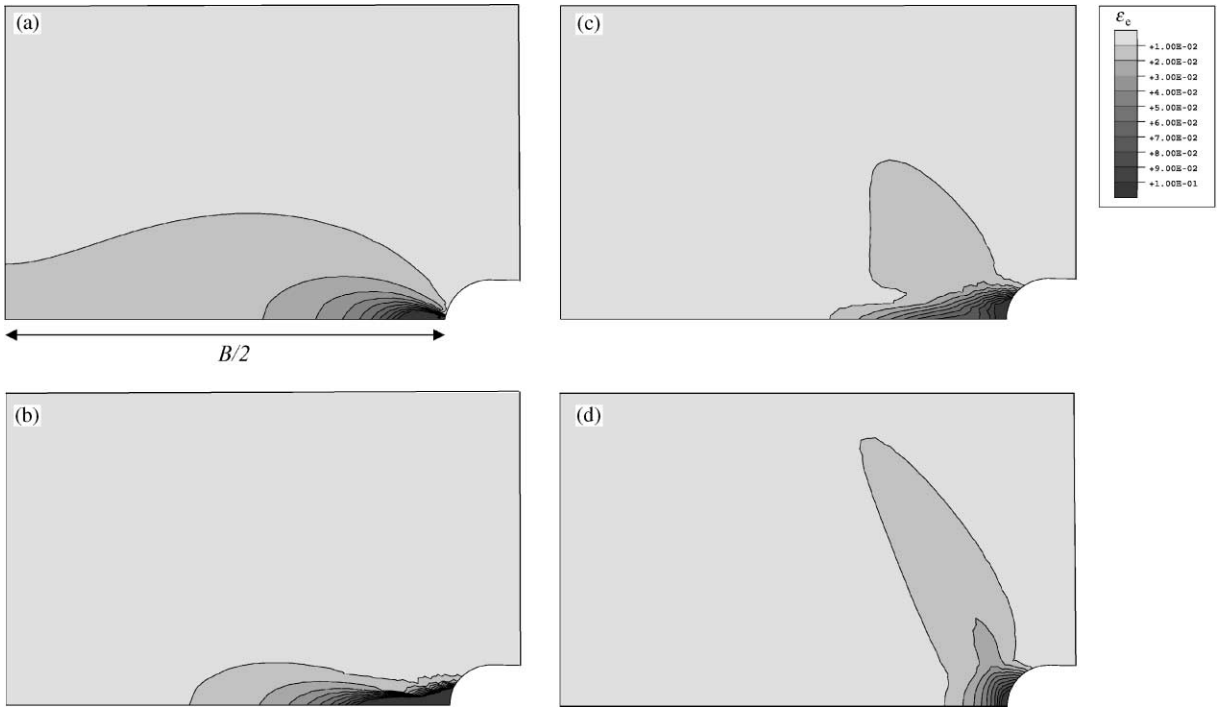

Fig. 6. Accumulated effective strain ε_e in the ligament region in front of the notch tip for $a/W = 0.5$ at an overall strain level of $\varepsilon = 0.0067$: (a) $\nu^p = 0$; (b) $\nu^p = 0.35$; (c) $\nu^p = 0.4$; (d) $\nu^p = 0.5$ (dense metal).

for $\nu^p = 0$, 0.3 and 0.5. The dashed lines as shown in Fig. 5a are omitted for clarity. It can be concluded that (13) captures the finite element results very well, showing that for $\nu^p < 0.3$ no substantial notch-strengthening occurs. Although not predicted by the finite element calculations, equation (13) even predicts notch-weakening for $a/W > 0.3$ when $\nu^p = 0$. Thus, given our model parameters, for incompressible materials the increased triaxiality due to the presence of a notch invariably leads to strengthening, related to constrained plastic deformation, while for foams with low ν^p the notch-strengthening is negligible, which is related to the hydrostatic stress dependence of yielding.

3.2. Deformation behavior

In this section, we focus on the local deformation patterns as a function of the plastic Poisson ratio for $a/W = 0.5$, taking, as in the previous section, $h/W = 1.5$ and $2\rho/W = 0.05$. Fig. 6 shows the accumulated effective strain ε_e, in the ligament region for $\nu^p = 0$, 0.35, 0.4 and 0.5 at an overall strain level of $\varepsilon = 0.0067$, which is right before the plateau stress has been reached (see Fig. 3). Clearly, Figs. 6a and b ($\nu^p = 0$ and 0.35, respectively) show that almost all deformation is concentrated in the elements in front of the notch tip in the symmetry plane. For $\nu^p = 0.4$ (Fig. 6c) the deformation pattern makes a switch from concentrated deformation in the symmetry plane to deformation under an angle, culminating in the $\nu^p = 0.5$ (Fig. 6d) case, where a clear shear-dominated deformation pattern has developed.

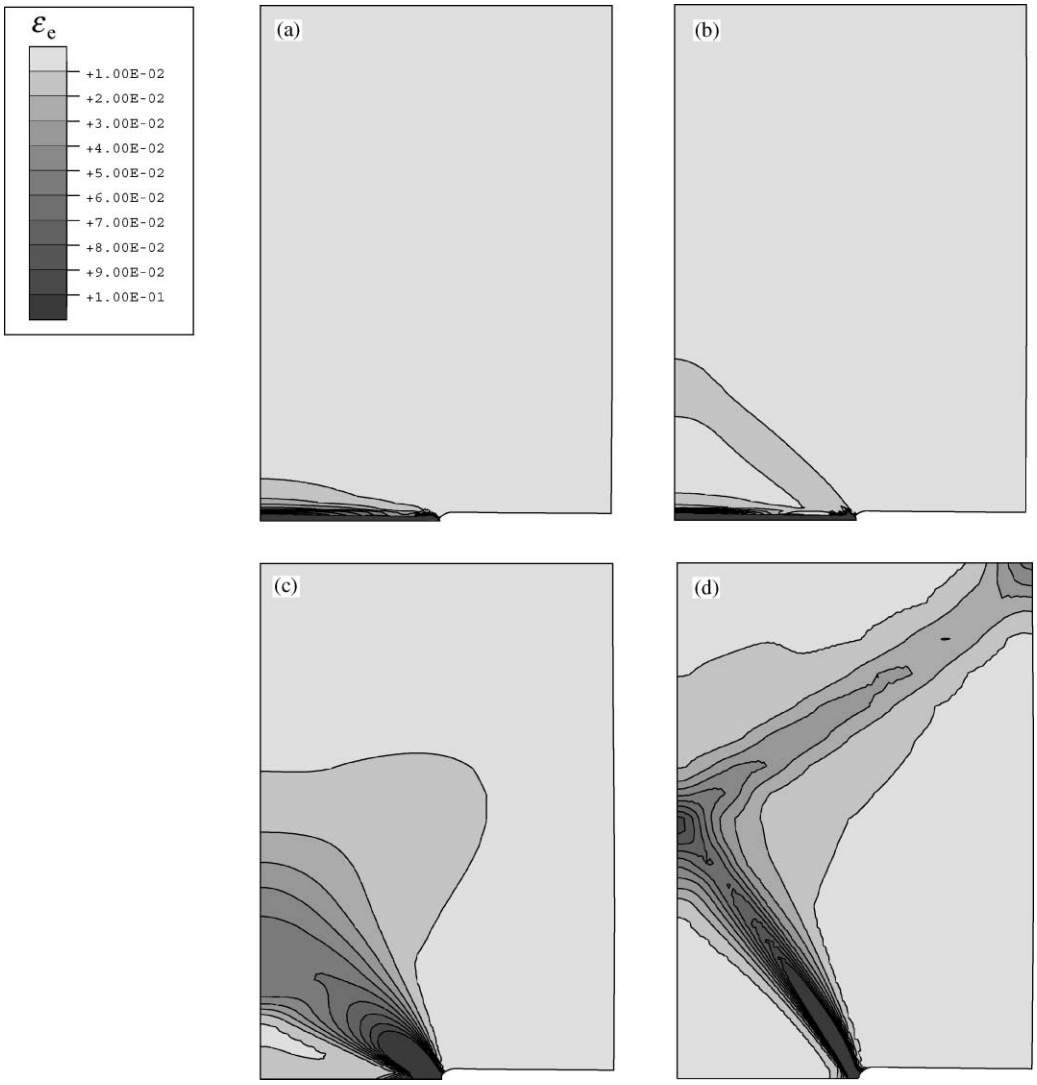

Fig. 7. Accumulated effective strain ε_e in the whole specimen for $a/W = 0.5$ at an overall strain level of $\varepsilon = 0.02$: (a) $v^p = 0.3$; (b) $v^p = 0.35$; (c) $v^p = 0.4$; (d) $v^p = 0.5$ (dense metal).

Next, we focus on the deformation patterns at an overall strain level $\varepsilon = 0.02$, which is after the plateau stress has been reached (see Fig. 3). Fig. 7 shows the accumulated effective strain ε_e, for $v^p = 0.3$, 0.35, 0.4 and 0.5 for the whole specimen, conform Fig. 2. The pattern of Fig. 7a is representative for $v^p \leqslant 0.3$, with all deformation concentrated in the symmetry plane, with a crushing mode being active. Crushing started at the notch tip (see e.g. Fig. 6a), where the plateau stress is reached earliest. After that, crushing spreads to neighboring material in the ligament. Note that by comparing Figs. 6b and 7b, 6c and 7c and 6d and 7d a clear picture can be obtained of the evolution of deformation. For $v^p = 0.35$ (Fig. 7b) it can be seen that some

strain has accumulated under an angle, but that still the horizontal crushing mode is dominant. At $\nu^p = 0.4$ and 0.5 (Figs. 7c and d, respectively) the deformation pattern changes to a shear-like mode, showing long-range interaction for $\nu^p = 0.5$ (dense metal).

4. Discussion

The compression of doubly edge notched specimens is analyzed by employing a phenomenological yield surface for metallic foams. The shape of the yield surface is elliptical in (σ_m, σ_e) space and depends on the plastic Poisson ratio ν^p. Results are presented in terms of limit load F_{lim} vs. notch depth a/W in addition to contour plots of the deformation patterns, for different values of the plastic Poisson ratio. For incompressible plastic behavior (dense metal, $\nu^p = 0.5$), the results show notch-strengthening due to constrained plastic deformation near the crack/notch tip. For fully compressible plastic behavior (no lateral expansion on uniaxial compression, $\nu^p = 0$), no notch-effect is observed.

Great care should be taken in comparing the present numerical results with experimental results obtained on lab specimens. Recently, Onck and Bastawros [16] performed such compression experiments on Alporas DEN-specimens with machined notches. The notch tip radius was approximately a half-cell size (cell size = 3.5 mm), leading to $2\rho/W = 0.06$, which is comparable to the numerical calculations. The experiments show a clear notch-strengthening behavior, while the experimental plastic Poisson ratio was observed to be very small, $\nu^p \approx 0$. Looking at the numerical results of Section 3 for the small plastic Poisson ratios (e.g. Fig. 5b) no dependence of F_{lim}/B on a/W was observed. This is clearly in contrast with the experimental results, which show an increased strength with a/W. The numerical results only predict similar notch-strengthening behavior for $\nu^p \approx 0.4$, which clearly does not correspond to low-density foamed materials. Moreover, if we take into account the actual dimensions of the specimens of the experiments, we observe that the notch is approximately one cell size high. Referring to Fig. 6, for instance, it is noted that the continuum constitutive model of Section 3.1 is applied at length scales much smaller than the material length (the cell size), which is in contradiction with the continuum assumption. This is the reason for the discrepancy between the experimental results and the numerical calculations for $\nu^p = 0$. To explain the experimentally observed notch-strengthening behavior, a microstructural model is needed that incorporates the material length scale properly, such that the interaction of individual cells in a non-uniform stress field can be accounted for. This can be achieved in a two-dimensional setting for instance by modelling the foam as a honeycomb, consisting of discrete cell walls (see e.g. [6,17]).

5. Concluding remarks

A continuum theory for metallic foams describes the average constitutive behavior of a representative volume element that is much larger than the microstructural length scale (the cell size). Therefore, by using a finite element model, each element is representative for a region consisting of many cells. In most commercial metallic foams, however, the cell size ranges from 2 to 6 mm, while typical specimen dimensions are of the order of 10 cell sizes. Clearly, for

these dimensions in regions of non-uniform stress fields, the continuum assumption is violated and a (local) continuum model as described here should not be used.

Acknowledgements

This research has been made possible by a fellowship of the Royal Netherlands Academy of Arts and Sciences.

References

[1] Deshpande VS, Fleck NA. Isotropic constitutive models for metallic foams. Journal of the Mechanics and Physics of Solids 2000;48:1253–83.
[2] Ashby MF, Evans AG, Fleck NA, Gibson LJ, Hutchinson JW, Wadley HG. Metal foams: a design guide. Oxford, UK: Butterworth-Heinemann, 2000.
[3] Gibson LJ, Ashby MF. Cellular solids. New York: Cambridge University Press, 1997.
[4] Simone AE, Gibson LJ. The effects of cell face curvature and corrugations on the stiffness and strength of metallic foams. Acta Materialia 1998;46:3929–35.
[5] Grenestedt JL. Influence of wavy imperfections in cell walls on elastic stiffness of cellular solids. Journal of the Mechanics and Physics of Solids 1998;46:29–50.
[6] Chen C, Lu TJ, Fleck NA. Effects of imperfections on the yielding of two-dimensional foams. Journal of the Mechanics and Physics of Solids 1999;47:2235–72.
[7] Sugimura Y, Meyer J, He MY, Bart-Smith H, Grenestedt J, Evans AG. On the mechanical performance of closed cell Al alloy foams. Acta Materialia 1997;45:5245–59.
[8] Bastawros A-F, Bart-Smith H, Evans AG. Experimental analysis of deformation mechanisms in a closed cell Al alloy foam. Journal of the Mechanics and Physics of Solids 2000;48:301–22.
[9] Triantafillou TC, Zhang J, Shercliff TL, Gibson LJ, Ashby MF. Failure surfaces for cellular materials under multiaxial loads—II: comparison of models with experiment. International Journal of Mechanical Sciences 1989;31:665.
[10] Gioux G, McCormack TM, Gibson LJ. Failure of aluminum foams under multiaxial loads. International Journal of Mechanical Sciences 2000;42:1097–117.
[11] Gibson LJ, Ashby MF, Zhang J, Triantafillou TC. Failure surfaces for cellular materials under multiaxial loads. I: Modeling. International Journal of Mechanical Sciences 1989;31:635–63.
[12] Zhang J, Lin Z, Wong A, Kikuchi N, Li VC, Yee AF, Nusholtz GS. Constitutive modeling and material characterization of polymeric foams. ASME Journal of Engineering Materials and Technology 1997;119:284.
[13] Miller RE. A continuum plasticity model for the constitutive and indentation behaviour of foamed metals. International Journal of Mechanical Sciences 2000;42:729–54.
[14] Akiyama S, Ueno H, Imagawa K, Kitahara AA, Nagata S, Morimoto K, Nishikawa T, Itoh M. Foamed metal and method of producing. US Patent 4, 713, 277, December 15, 1987.
[15] Chen C. Manual for a UMAT user subroutine. Technical Report CUED/C-MICROMECH/TR. 4, 1998, Dept. of Engineering, University of Cambridge.
[16] Onck PR, Bastawros A-F. The characteristics of notch effects in a closed-cell Al alloy foam. 2001, in preparation.
[17] Guo XE, Gibson LJ. Behavior of intact and damaged honeycombs: a finite element study. International Journal of Mechanical Sciences 1999;41:85–105.